

RSC Advances



This is an *Accepted Manuscript*, which has been through the Royal Society of Chemistry peer review process and has been accepted for publication.

Accepted Manuscripts are published online shortly after acceptance, before technical editing, formatting and proof reading. Using this free service, authors can make their results available to the community, in citable form, before we publish the edited article. This *Accepted Manuscript* will be replaced by the edited, formatted and paginated article as soon as this is available.

You can find more information about *Accepted Manuscripts* in the [Information for Authors](#).

Please note that technical editing may introduce minor changes to the text and/or graphics, which may alter content. The journal's standard [Terms & Conditions](#) and the [Ethical guidelines](#) still apply. In no event shall the Royal Society of Chemistry be held responsible for any errors or omissions in this *Accepted Manuscript* or any consequences arising from the use of any information it contains.



Journal Name

ARTICLE

Conformational ensembles of neuromedin C reveal a progressive coil-helix transition within a binding-induced folding mechanism

Miquel Adrover,^{*a,b} Pilar Sanchis,^{a,b} Bartolomé Vilanova,^{a,b} Kris Pauwels,^{c,d} Gabriel Martorell,^e and Juan Jesús Pérez^f

Received 00th January 20xx,
Accepted 00th January 20xx

DOI: 10.1039/x0xx00000x

www.rsc.org/

Neuromedin C (NMC) is a peptide that regulates various processes in the central nervous system and gastrointestinal tract through its interaction with the bombesin receptor subtype-2 (BB₂R). Hence, BB₂R antagonists hold potential to treat disorders that occur as a result of NMC dysfunction or misregulation. However, their efficient design requires a detailed understanding of the structural features of NMC, which hitherto are unknown. Here we describe the conformational ensembles of NMC in aqueous solution, at five different TFE concentrations to decode its folding pathway, and under its SDS micelle bound state. NMC displays a disordered but well-defined backbone architecture that undergoes a progressive coil-helix transition with increasing TFE concentrations, first at the C-terminus and then at the N-terminus. NMC also adopts a C-terminal α -helical conformation upon binding to SDS micelles. This micelle binding is directed by hydrophobic interactions that concur with the unfavorable deprotonation of His⁸ and its further insertion into the micelle. Moreover, NMR relaxation data reveal that the acquisition of the micelle bound α -helical conformation constrains the NMC flexibility more than the confinement itself. This comprehensive study of the structural behavior of NMC provides essential mechanistic information that could be useful for the development of new therapeutics to treat neurological, cancer-related or eating disorders.

1 Introduction

Neuromedin C (NMC) is an endogenous decapeptide (GNHWAVGHLM-NH₂) that is highly conserved in mammals.¹ It exerts a variety of biological effects both on the central nervous system (CNS) and in the gastrointestinal tract.¹ Together with gastrin-releasing peptide (GRP) and neuromedin B (NMB), NMC belongs to the bombesin-like peptide family. Bombesin is a 14-residue peptide originally isolated from the amphibian *Bombina bombina*.² As well as its two mammalian analogues (GRP and NMB), NMC functions as a neurotransmitter, paracrine hormone, growth factor and it retains the full hormone activity of GRP.³

NMC exerts its physiological function mainly by its interaction with the subtype-2 bombesin receptor (BB₂R), which is a member of the G-protein coupled receptor superfamily⁴ that is located in the gut

and in the CNS.⁵ For instance, NMC mediates neurotransmission and neuromodulation,⁶ and it is able to excite specific neurons by decreasing the resting potassium conductance and increasing the non-specific conductance.⁷ NMC can also reduce the appetite, and therefore can act as anorexia inducer,⁸ likely through its interaction with bombesin receptors in the central amygdala.⁹ In addition, its intravenous administration increases growth hormone levels in calves,¹⁰ while it can also act as an autocrine growth factor in human small-cell lung cancer.¹¹ Moreover, NMC has been shown to regulate growth and/or differentiation of human tumors in a wide range of tissues including carcinomas of pancreas, stomach, breast, prostate and colon.¹² Accordingly, a novel protein vaccine consisting of six covalently linked repeats of NMC was successful in suppressing the proliferation of breast tumor cells.¹³

As a result of NMC's pharmacological profile, BB₂R antagonists are considered as prospective anticancer therapeutics¹⁴ and for the treatment of other illnesses.¹⁵ RC-3095, a peptidomimetic of NMC, was shown to produce long-lasting tumor regressions in different human models,¹⁶ as well as to show beneficial effects during the treatment of tumor necrosis factor-dependent chronic inflammatory conditions.¹⁷ More recently, a N-terminal modified NMC with acyclic tetraamines for binding of ^{99m}Tc ([^{99m}Tc-Demomedin C) was successfully targeted in BB₂R expressing tumor cells as a potent agonist inducing selective intracellular calcium release and triggering GRP receptor mediated internalization of the radioligand.¹⁸ However its tolerability, background radioactivity and retention in tumor lesions warrant future studies as these pharmacological aspects have led to the rejection of other ^{99m}Tc-bombesin analogs.¹⁹

^a Institut Universitari d'Investigació en Ciències de la Salut (IUNICS). Departament de Química, Universitat de les Illes Balears (UIB), Ctra. Valldemossa km 7.5, E-07122, Palma de Mallorca (Spain). E-mail: miquel.adrover@uib.es

^b Instituto de Investigación Sanitaria de Palma (IDISPA), Ctra. Valldemossa, 79, E-07010, Palma de Mallorca (Spain)

^c Structural Biology Brussels, Vrije Universiteit Brussels (VUB), Pleinlaan 2, 1050 Brussels (Belgium)

^d Structural Biology Research Centre, Vlaams Instituut voor Biotechnologie (VIB), Pleinlaan 2, 1050 Brussels (Belgium)

^e Serveis Científic-Tècnics, Universitat de les Illes Balears (UIB), Ctra. Valldemossa km 7.5, E-07122, Palma de Mallorca (Spain)

^f Departament d'Enginyeria Química, Universitat Politècnica de Catalunya (UPC), ETSEIB, Av. Diagonal, 647, E-08028, Barcelona (Spain)

† Footnotes relating to the title and/or authors should appear here.

Electronic Supplementary Information (ESI) available. See

DOI: 10.1039/x0xx00000x

The efficient design of more potent antagonists of BB₂R requires a detailed understanding of the structure-activity relationships of NMC. However, very limited structural information on NMC is currently available. In contrast to bombesin or NMB, NMC was predicted not to adopt a α -helical conformation upon binding to non-polar sites, due to reduced hydrophobic interactions that arise from the replacement of Leu³ by His³ in NMB.²⁰ Yet, Polverini et al. used CD spectroscopy to suggest that NMC could adopt a helical-like conformation upon binding to lipids.²¹ Later NMR spectroscopy was applied to solve the solution structure of the NMC-Ni²⁺ complex that consists of two connected turns,²² also likely adopted in the NMC-Cu²⁺ complex that could be physiologically involved in metal transport along the CNS.²³ More recently we have used replica exchange molecular dynamics (REMD) to demonstrate that NMC, in a simulated aqueous environment, adopts different conformations resembling β -turns that are stabilized by different hydrogen bonds formed and broken along the trajectory.²⁴

Although computer simulations can reveal the intrinsic conformational features of a peptide as encrypted in its sequence, caution should be taken about the thoroughness of the sampling. Therefore, we aim here to complete these preliminary computational results with further structural evidences. We have combined different biophysical techniques to study the conformational ensemble of NMC in aqueous solution, and at five different 2,2,2-trifluoroethanol (TFE)/water percentages (i.e. at 10, 25, 40, 60 and 90% TFE). As TFE typically can induce α -helicity in polypeptides,²⁵ we complemented these data by analyzing the α -helical structure of NMC bound to SDS micelles, characterizing the NMC-SDS micelle complex, and evaluating independently the structuring and the binding effects on the peptide flexibility. These data constitute a comprehensive overall picture about the conformational preferences of NMC under different environments, and represents a new structural platform for the future development of BB₂R antagonists.

2 Results

2.1 NMC is an intrinsically disordered peptide that undergoes a progressive coil-helix transition upon increasing TFE concentration

It is already described that NMC displays a native random coil conformation in aqueous solution.²¹ However, so far no experimental insight describes how the NMC conformation changes upon varying the dielectric environment, as might occur when it binds to the BB₂R. Hence, we approached this folding process by studying the effect of increasing TFE concentrations on the NMC conformation. TFE has been widely used as a kosmotropic agent to study protein folding.²⁵ Moreover, it has a low effect on the pH of acetate buffered solutions when it is added up to 90% ($\Delta\text{pH}\sim 0.4$),²⁶ which makes it highly suitable for our study.

The CD spectrum of NMC in aqueous solution indicates that the peptide is disordered, as evidenced by the minimum located at 197nm. A slight increase in the TFE percentage, from 0 to 10%, scarcely modifies the spectrum profile as well as the secondary structure content. However, the addition of TFE at percentages higher than 10% markedly enhances the intensity of the region between 190-202nm and reduces that of the band located between 206-240nm, which turns into a notable increase of the α -helical

content while decreasing the percentages of β -strands, turns and random coil regions (**Figure 1A** and **Table S1**).

These results indicate that NMC adopts a predominant α -helix conformation upon addition of TFE, but only when the percentages are higher than 10%.

2.2 The Trp⁴-Gly⁷ region holds the higher α -helicity tendency

Although CD spectroscopy provided general information on the folding behavior of NMC upon increasing the TFE/water ratios, it does not give any insight at the residue level on how the structuring process occurs. Therefore, we carried out the NMR study of NMC at different TFE/water ratios. The ¹H-, ¹⁵N- and ¹³C-NMR assignments were obtained at 15°C for different NMC solutions containing 0, 10, 25, 40, 60 or 90% TFE. Chemical shifts of the backbone atoms (i.e. N, HN, H α and C α) were obtained for all residues, except those corresponding to the N and the HN of Gly¹ (that could not be achieved at any TFE percentage) and Asn² (which could only accomplish at 0, 10 and 25% TFE). The C α resonance of Asn² at 40% TFE could neither be observed. All the N, H and C atoms at the side chains were assigned. The chemical assignments of NMC have been deposited to BMRB under the accessions codes 25519 (0% TFE), 25520 (10% TFE), 25521 (25% TFE), 25522 (40% TFE), 25523 (60% TFE) and 25524 (90% TFE).

Chemical shifts corresponding to H_N, N, H α , H β , C α and C β were used to determine the secondary structural propensity (SSP) scores (see section 4.5) at different TFE/water ratios (**Figure 1B**). The obtained SSP plots suggest that the structures of NMC at 0 and 10% TFE are similar, except for the residues located at the C-terminus, which seem to slightly enhance their helicity at 10% TFE. While both structures seem to be random coil, the increase in the TFE percentage above 10% clearly induces an enlargement of the α -helix content, which is more prominent in the central region of the peptide (Trp⁴-Gly⁷). On the other hand, most of the SSP values obtained at 90% TFE are higher than 0.5, which indicates that the corresponding residues display a well-defined α -helical structure.

These results are in agreement with the CD data, and prove that the peptide central region (Trp⁴-Gly⁷) holds the higher α -helical tendency.

2.3 The folding pathway of NMC upon increasing the TFE concentration

The ¹H-, ¹⁵N- and ¹³C-NMR assignments were used to calculate the solution structures of NMC at each TFE/water ratio. The geometrical restraints used during the calculations were taken from the NOEs intensities and automatically assigned using the CYANA software²⁷ (**Figure S1**). These assignments provided NMR ensembles with all dihedral angles located in favored and allowed regions, and with low backbone RMSD, except for the most disordered NMC structures obtained at 0 and 10% TFE. The obtained ensembles have been deposited to PDB under the accessions codes 2n0b (0% TFE), 2n0c (10% TFE), 2n0d (25% TFE), 2n0e (40% TFE), 2n0f (60% TFE) and 2n0g (90% TFE), and all of them satisfy all convergence criteria for successful structure calculations (**Table 1**).

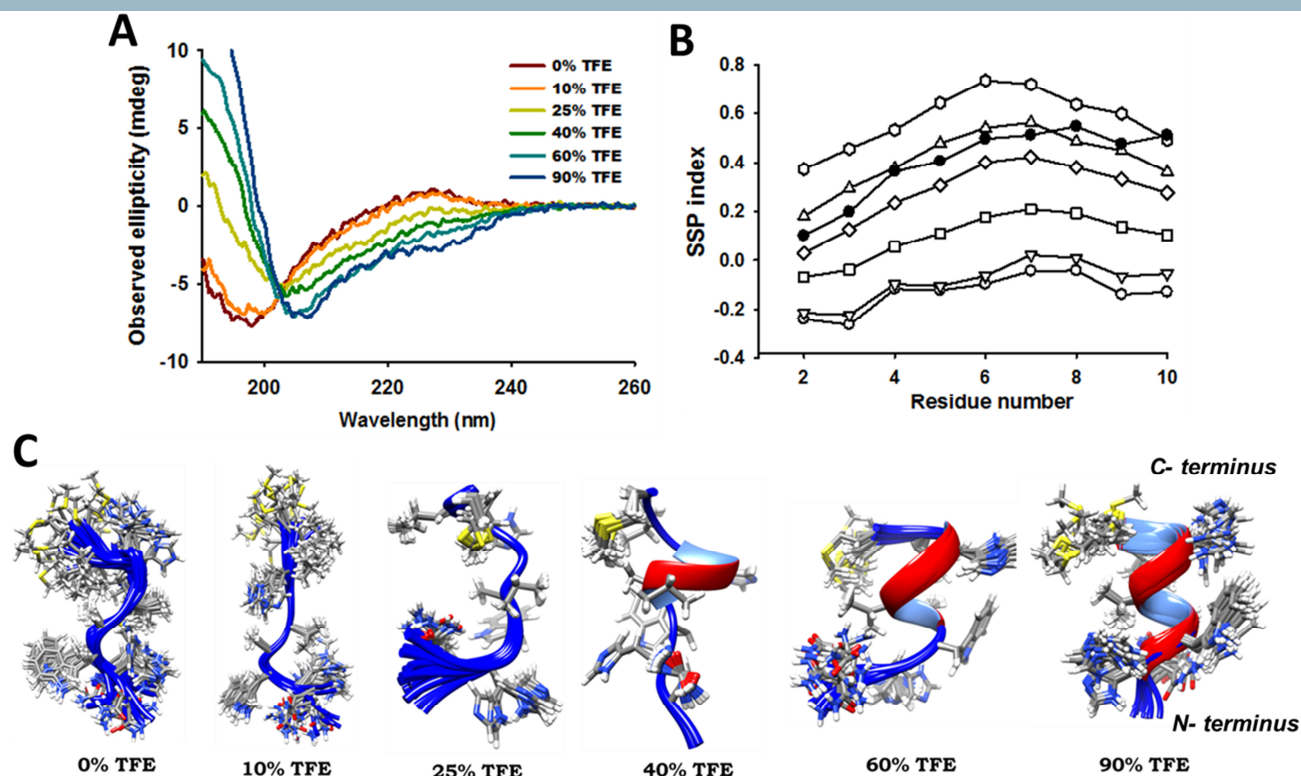


Figure 1. Analysis of the NMC conformation under different experimental conditions. (A) CD spectra of NMC in the presence of different percentages of TFE in 10mM acetate buffer (pH 4.0) at 15°C. (B) SSP values of NMC, as calculated from $^1\text{H}_\text{N}$, ^{15}N , $^1\text{H}_\alpha$, $^1\text{H}_\beta$, $^{13}\text{C}_\alpha$ and $^{13}\text{C}_\beta$ chemical shift values at pH 4.0 and 15°C at 0% (●), 10% (▽), 25% (□), 40% (◇), 60% (△) and 90% (◊) of TFE, and in the presence of 150mM SDS (●). (C) NMR solution ensembles of the ten lowest energy structures of NMC calculated at different TFE/water ratios in 10mM acetate buffer (pH 4.0) at 15°C. Backbone atoms are represented as ribbons, while the side chains are shown as atom colored sticks. Images were generated using the UCSF Chimera software.

Table 1. Structural statistics for the different conformers of NMC obtained at different d_3 -TFE/water ratios and in the presence of d_25 -SDS micelles							
	0% TFE	10% TFE	25% TFE	40% TFE	60% TFE	90% TFE	SDS
Structural computed conformers	18	17	20	20	19	20	20
Restraints^[a]							
Short-range ($ i-j \leq 1$)	47	71	91	121	80	79	99
Medium-range ($1 < i-j < 5$)	3	2	23	49	24	35	39
Long-range ($ i-j \geq 5$)	0	0	2	7	3	0	0
NOE constrains per restrained residue	7.1	9.0	12.8	19.3	13.1	12.1	13.8
Torsion angles restraints	0.0	0.0	0.0	0.0	0.0	0.0	0.0
Restraints statistics^[b]							
Distance violations $> 0.0 \text{ \AA}$	5	4	3	4	2	3	2
Torsion angle violations $> 0^\circ$	0	0	0	0	0	0	0
Target function value (\AA^2)							
Average/best	0.0	0.0	0.02	0.0	0.02	0.0	0.0
Pairwise RMSD of residues 3-8 in \AA^[c]							
Backbone N, CA, C'	0.73 \pm 0.26	0.63 \pm 0.29	0.08 \pm 0.07	0.01 \pm 0.00	0.06 \pm 0.04	0.25 \pm 0.1	0.17 \pm 0.7
Heavy atoms	1.87 \pm 0.51	1.40 \pm 0.38	0.43 \pm 0.30	0.05 \pm 0.01	0.41 \pm 0.20	1.05 \pm 0.32	0.57 \pm 0.35
Ramachandran plot^[d]							
Most favoured regions (%)	54.8	47.1	47.9	55.0	75.7	82.9	60.7
Additional allowed regions (%)	45.2	52.9	52.1	45.0	23.4	17.1	39.7
Generously allowed regions (%)	0.0	0.0	0.0	0.0	0.0	0.0	0.0
Disallowed regions (%)	0.0	0.0	0.0	0.0	0.0	0.0	0.0

^[a] Restraint statistics reported for unique, unambiguous assigned NOEs.
^[b] Violations are only reported when present in six or more structures.
^[c] Coordinate precision is given as the average pair-wise cartesian coordinate root mean square deviations over the ensemble.
^[d] Values obtained from the PROCHECK-NMR analysis⁶⁸ by using the Protein Structure Validation Server (PSV).⁶⁹

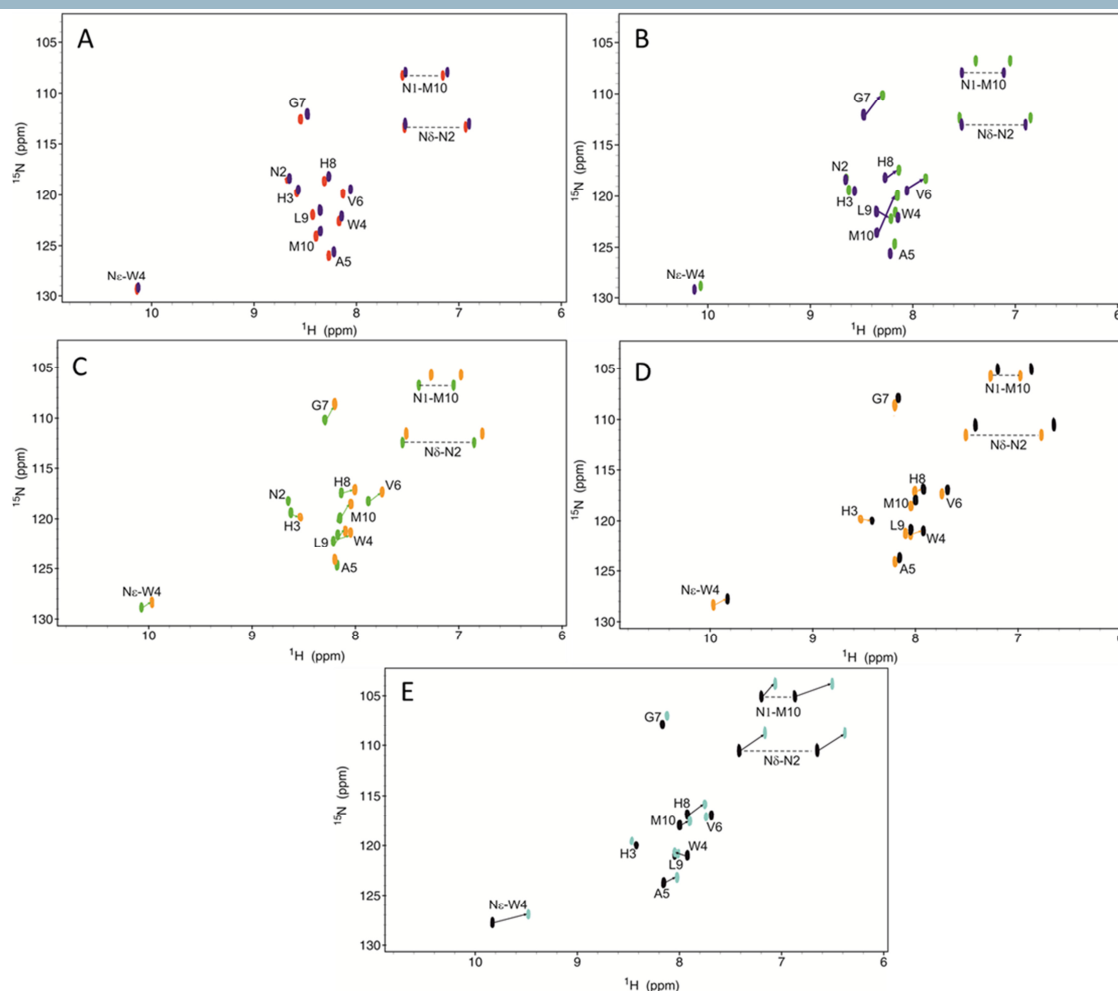


Figure 2. Overlapping of the ^{15}N -HSQC spectra of NMC obtained at different d_3 -TFE/water ratios. (A) ^{15}N -HSQC spectra of NMC in presence of 0% (red) and 10% (purple) TFE. (B) ^{15}N -HSQC spectra of NMC in presence of 10% (purple) and 25% (green) TFE. (C) ^{15}N -HSQC spectra of NMC in presence of 25% (green) and 40% (orange) TFE. (D) ^{15}N -HSQC spectra of NMC in presence of 40% (orange) and 60% (black) TFE. (E) ^{15}N -HSQC spectra of NMC in presence of 60% (black) and 90% (cyan) TFE. The arrows indicate the cross-peak shift from the lower to the higher TFE percentage.

The NMC ensemble calculated in aqueous solution displays a native random coil conformation. Nevertheless, the corresponding backbone RMSD is lower than that expected for a fully unstructured ensemble, mostly as a result of the short range NOEs detected between central amino acids, which create a backbone architecture resembling a distorted *S* (Figure 1C).

The NMC structure obtained at 10% TFE does not differ significantly to that found in water, which is in perfect agreement with previously reported CD and SSP data (Figures 1A,B). However, while the depicted *S*-like conformation between His³-His⁸ is still preserved, the C-terminal region appears to adopt a more extended structure (Figure 1C). This subtle but remarkable difference was already revealed by the SSP data, but it can also be observed from the overlapping of the ^{15}N -HSQC spectra of NMC at 0 and 10% TFE,

where the chemical shift perturbations of Val⁶, Gly⁷ and Leu⁹ are larger than those of Asn², His³, Trp⁴ or Ala⁵ (Figure 2A).

CD and SSP data already suggested that an increase in the TFE content from 10 to 25% implies a larger structural rearrangement than that occurring when the TFE percentage rises from 0 to 10%. Moreover, the overlapping of the ^{15}N -HSQC spectra obtained at 10 and 25% TFE additionally shows that this rearrangement mainly occurs at the C-terminus, as is evidenced by the chemical shift perturbations displayed by the Val⁶-Met¹⁰ stretch (Figure 2B). The NMC structure obtained at 25% TFE does not exhibit the *S*-like conformation observed at 0 and 10% TFE. In contrast, residues at the C-terminus (up to Trp⁴) roll up and adopt a helical-like turn, whereas the N-terminal region bends back towards the central residues (Figure 1C).

The NMC solution structure obtained at 40% TFE shows the formation of a short but well defined α -helix at the C-terminus (Ala⁵-His⁸) as a result of an increased compactness of the structure displayed at 25% TFE (Figure 1C). On the other hand, the N-terminal region remains unstructured, but adopts a newly extended conformation. Therefore, the increase in the TFE percentage from 25 to 40% implies an overall structural rearrangement that is also evident from the comparison of the corresponding ¹⁵N-HSQC spectra, where the entire resonances shift (Figure 2C).

At 60% TFE the chemical shifts of the residues comprised between Val⁶-Met¹⁰ do not show remarkable differences in comparison with those obtained at 40% TFE. However, more noticeable are the shifts of the cross-peaks corresponding to His³ and Trp⁴ (Figure 2D). These variations result from the preservation of the α -helical structure between Ala⁵-His⁸ already formed at 40% TFE, whereas the residues at the N-terminus fold back also adopting a new α -helical conformation (Figure 1C).

The increase in the TFE percentage mostly resulted in an overall chemical shift variation of the ¹H-¹⁵N cross-peaks towards high field, especially in the ¹H dimension (Figure 2), which can be attributed to the lower capacity of TFE to form hydrogen bonds relative to water.²⁸ This was also the case when the TFE percentage rose from 60 to 90%, except for His³ and Trp⁴, whose cross-peaks shifted towards low field, suggesting a further structural rearrangement at the N-terminus (Figure 2E). The structure of NMC obtained at 90% TFE evidences an enlargement of the Ala⁵-His⁸ α -helical stretch depicted at 60% TFE towards Leu⁹, but also towards Trp⁴ and His³ (Figure 1C). Hence, the compacter conformation adopted by the N-terminus when going from 40 to 60% TFE, becomes fully α -helical at 90% TFE.

Thus, NMC is a disordered peptide in aqueous solution, although its central region exhibits a constrained backbone architecture resembling a distorted S. Upon increasing TFE/water ratios the C-terminal region first stretches to fold back into an α -helical structure, which also occurs at the N-terminus but only at higher TFE percentages.

2.4 NMC binds to SDS micelles

TFE is known to induce α -helicity in most polypeptides through a process that mimics their embedding into regions of low dielectric constant and high viscosity.²⁵ Hence, the use of different TFE/water ratios allowed the modelling of a folding route that could mimic that occurring during its interaction with the BB₂R.

Additionally we have complemented these results by studying the biophysical characteristics of NMC upon interaction with SDS micelles, which were chosen as a model system.

We ran diffusion-oriented (DOSY) NMR experiments on a solution containing NMC alone or in presence of SDS micelles. The resulting diffusion coefficients (*D*) were independent of the NMC concentration, indicating that no self-aggregation occurred in both samples. Assuming that the slight viscosity change linked to the presence of SDS micelles equally affects the reference (i.e. acetate and DSS signals) and the NMC signals, it is clear NMC reduces its

overall mobility in presence of SDS micelles (Figure 3A), which potentially suggest their binding.

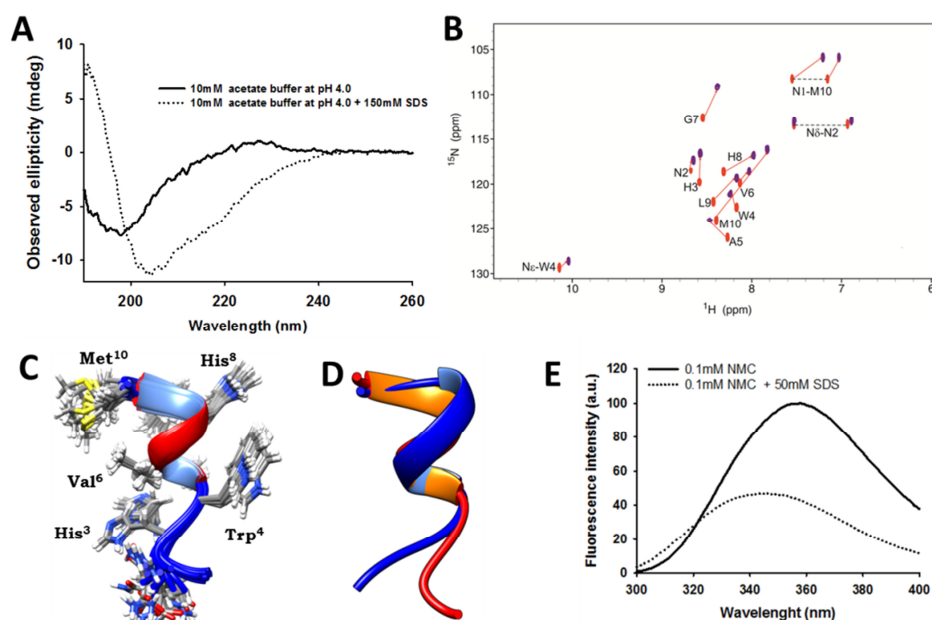
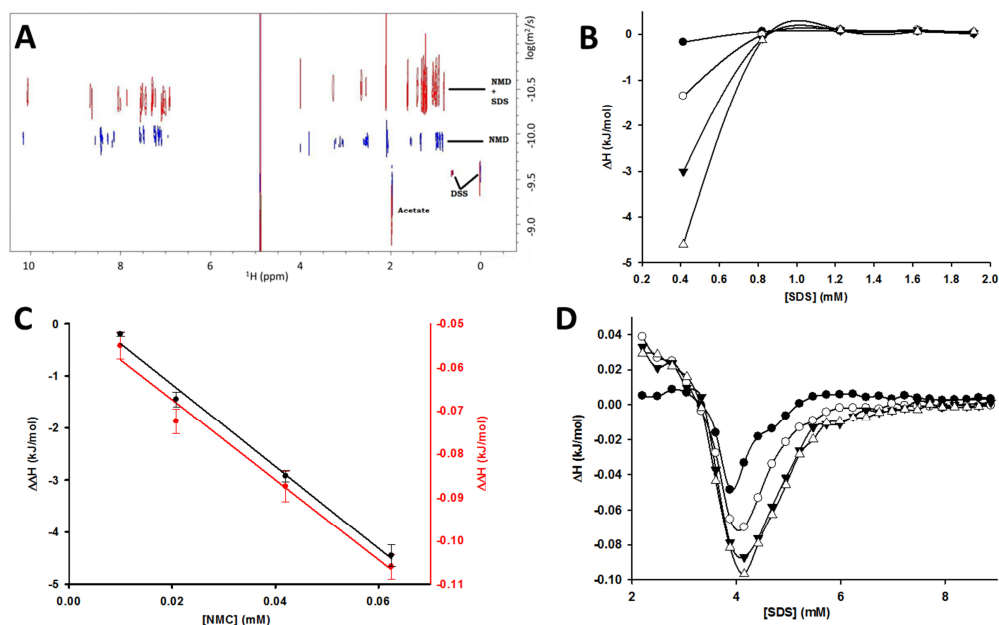
ITC was then used to thermodynamically characterize the binding process. The titration curve of SDS in acetate buffer resulted in the appearance of initial exothermic peaks accounting for the low-temperature energy favored demicellization.²⁹ These peaks became less exothermic as they approached to the midpoint of the inflection (critical micelle concentration; *cmc*),³⁰ to finally become endothermic as a result of the micelle dilution effect²⁹ (Figure S2).

A similar trend was observed when titrations were carried out on solutions containing NMC (Figure S2). However, several differences ascribable to the SDS-NMC interaction were observed. Difference enthalpograms reveal an initial exothermic heat flow that rapidly levels off as SDS concentration increases (Figure 3B). This effect likely corresponds to specific and cooperative electrostatic interactions occurring between the SDS-sulfate group and cationic His.³¹ The amplitude of this variation scales linearly with NMC concentration (Figure 3C) and the obtained slope ($\alpha_{\Delta H} \sim -79 \pm 5$ kJ/mol·mM) indicates that there is a big change in the ΔH of the system upon a small change in both protein and surfactant [$\alpha_{\Delta H}$ is proportional to $(d^2H)/(dn_{\text{protein}}dn_{\text{SDS}})$ and measures the enthalpy of NMC-SDS interaction³²].

Next, the enthalpy difference became slightly endothermic, which could be attributed to a conformational rearrangement of NMC.³³ Then the curves began to deviate exothermically from the control curve at a SDS concentration of ~ 3.3 mM, which corresponds to the onset for binding of NMC to SDS (critical aggregation concentration; *cac*).³⁴ The subsequent exothermic variation is attributed to the association of SDS and NMC,³³ whose saturation is at the inflection point and corresponds to the *cmc*, which slightly increases with the NMC concentration (3.9-4.2 mM). SDS injected beyond this point remains in micellar form, having fewer NMC molecules to interact, and leading to the final asymptotic curve (Figure 3D). The amplitude of this curve linearly scales with NMC concentration and the obtained $\alpha_{\Delta H} \sim -0.92 \pm 0.09$ kJ/mol·mM (Figure 3C) proves that the nature of the interaction between SDS micelles and NMC is much weaker than an electrostatic one.

Cac and *cmc* values were additionally used to calculate the Gibbs free energy changes of aggregation (ΔG_{mic}) and the Gibbs free energy changes of aggregation in presence of NMC (ΔG_{ag}) through the application of the charged phase separation and mass-action model.³⁵ The obtained ΔG_{mic} and ΔG_{ag} values were -24 ± 2 and -25 ± 1 kJ/mol respectively, which proves that the micellar behavior of SDS and the formation of NMC/SDS mixed micellar junctions are both similarly thermodynamically favored. Moreover, the ΔH_{mic} and ΔH_{ag} , both < -0.1 kJ/mol (Figure 3D), are much smaller than the terms $T\Delta S_{\text{mic}}$ or $T\Delta S_{\text{ag}}$ (~ 24 kJ/mol) revealing that both the aggregation of SDS in the absence and in the presence of NMC is entropy driven.

According to Lindman and Thalberg,³⁵ the free energy to drive 1 mol of monomeric SDS into NMC-bound micelle ($\Delta G_{\text{ps}} = \Delta G_{\text{ag}} - \Delta G_{\text{mic}}$) is indicative of the binding strength of SDS onto NMC. The obtained $\Delta G_{\text{ps}} \sim -1$ kJ/mol reveals that the binding between NMC-SDS is only slightly thermodynamically favored in comparison to that occurring between SDS-SDS molecules.





2.5 Solution structure of NMC bound to SDS micelles

Upon showing that NMC binds to SDS micelles, we wanted to assess this binding effect on the peptide structure. In contrast to bombesin or NMB, NMC was predicted not to adopt a membrane-inserted α -helical conformation due to the reduction of hydrophobic interactions upon replacement of Leu³ by His³, which would be needed to build effectively the α -helix.²⁰ However, the CD spectrum of NMC bound to SDS micelles indicated the contrary: the presence of micelles induced a redshift in the minimum, while the intensity of the regions between 191-193nm and 200-240nm increased and decreased respectively (**Figure 4A**). This indicates that NMC increases its α -helicity upon binding to SDS micelles at content similar to that shown at 60% TFE (**Table S1**).

NMR was then used to obtain residue level insights on this helical rearrangement. The comparison of the ¹⁵N-HSQC spectra of NMC obtained in the absence and in the presence of d₂₅-SDS show notably chemical shift perturbations as a result of the binding. This occurs for all residues except for the cross-peaks of Asn² (i.e. HN-N and HN⁶-N⁶), which indicates that the chemical environment of Asn² is only slightly modified upon micelle interaction (**Figure 4B**). All ¹H, ¹⁵N, and ¹³C resonances (except those for N and HN of Gly¹) were unambiguously assigned, deposited to BMRB (25525), and used to calculate the SSP values, which were also comparable to those obtained at 60% TFE (**Figure 1B**). Hence, CD and SSP data strongly suggest that the structure of NMC bound to SDS micelles must be similar to that obtained at 60% TFE.

The geometrical restrains automatically obtained from the NMR assignment and the ¹H-¹H-NOE intensities (**Figure S1**) were used to calculate the solution structure of NMC bound to d₂₅-SDS micelles. The obtained ensemble, deposited to the PDB under the accession code 2n0h, has an excellent Procheck-NMR score satisfying all convergence criteria for structure calculations (**Table 1**). The obtained structure reveals that the binding process induces the formation of an α -helical stretch between Ala⁵-Leu⁹, while the N-terminus retains the native random coil conformation (**Figure 4C**). In fact, this structure is very similar to that obtained in 60% TFE, which is ascertained by the low RMSD value arising from the alignment of the averaged structures of both ensembles (0.52Å for the backbone atoms) (**Figure 4D**).

Our results show that NMC binds to SDS micelles through a process that implies the formation of an α -helical stretch at the C-terminus, while the N-terminal segment remains disordered.

2.6 Trp⁴ is embedded into the SDS micelle

We then wanted to understand the molecular architecture of the complex formed between NMC and SDS micelles. Initially we used fluorescence spectroscopy to determine whether Trp⁴ is inserted

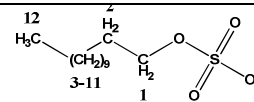
into the micelles. The fluorescence spectrum of NMC shows an emission maximum at 356 nm, typical of a solvent exposed indole group. However, when NMC binds to SDS micelles the fluorescence maximum undergoes to a hypsochromic shift, from 356 to 345nm, suggesting the incorporation of the Trp⁴ side chain into a less polar environment (**Figure 4E**). Conversely, the quantum yield of Trp⁴ also decreases in agreement with what was found during other peptide-SDS micelle interactions.³⁶

The extent to which Trp⁴ was buried into the micelles was determined using acrylamide quenching experiments. Equal amounts of acrylamide were added to solutions containing either free NMC or NMC-SDS micelles complex. The presence of micelles decreased approximately three times the Stern-Volmer constant (K_{sv}) of NMC ($\sim 13M^{-1}$ for the free form vs. $\sim 4M^{-1}$ for the complex) (**Figure S3**), indicating a high degree of protection of Trp⁴ side chain against the solvent. Hence, Trp⁴ side chain inserts into the SDS micelles during the binding process.

2.7 Mapping the interactions between NMC and SDS micelles

The atomic contact map between NMC and SDS micelles was obtained from the overlapping of the ¹H,¹H-NOESY spectra obtained in presence of 150mM d₂₅-SDS and in presence of 50mM SDS. The change in the SDS concentration did not alter the NMC structure, as evidences the comparison of both ¹⁵N-HSQC spectra (**Figure S4**).

Table 2. NOE connectivities found between NMC and SDS micelles.^[a]

NMC			
	CH ₂ (1) ^[b]	CH ₂ (2) ^[b]	CH ₂ (3-11) ^[b]
H _N -V6			++
H _N -L9			+
H _N -M10			+
H _α -W4			++
H _α -A5			++
H _α -V6			++
H _α -L9			+
H _{β2} -W4			+
H _{β3} -W4	++		++
H _{β3} -H8			+
H _{β3} -M10	+		
H _{γ2} -M10	+		
H _{ε1} -W4	+	+	++
H _{ε3} -W4		+	++
H _{ζ2} -W4	+		++
H _{δ1} -W4	+	+	++
H _{δ3} -W4		+	+++
H _{δ2} -H8			++
H _{γ1} -V6	++		
H _{γ2} -V6	++		

^[a]The intensities of the NOEs signals are divided as: "+++" high intensity; "++" medium intensity; "+" low intensity.

^[b]Atoms are numbered arbitrarily according the chemical structure of SDS.

The use of non-deuterated SDS resulted in the appearance of new NOEs that were unambiguously assigned to specific intermolecular NMC-SDS contacts. The side chain of Trp⁴ is fully embedded into the SDS micelles since its indol group exhibits strong NOEs with different SDS methylene groups. In addition, the HN of Val⁶, Leu⁹ and Met¹⁰, as well as the H_α of Trp⁴, Ala⁵, Val⁶ and Leu⁹ display different NOEs with the aliphatic tail of SDS, proving that the backbone at the C-terminus is also inserted into the SDS micelles. NOEs signals connecting the Val⁶ and Met¹⁰ side chains with protons

of C1 in SDS were also found, indicating that these regions protrude from the hydrophobic core of the micelle (Figure 5A and S5)(Table 2).

When analyzing the structure of NMC upon binding to SDS micelles (Figure 4C), it is difficult to understand how this interaction can occur since an amphipathic-like architecture is lacking. For instance, His⁸ points towards the same face of the helix than Trp⁴, while His³, Val⁶ and Met¹⁰ are in the opposite one.

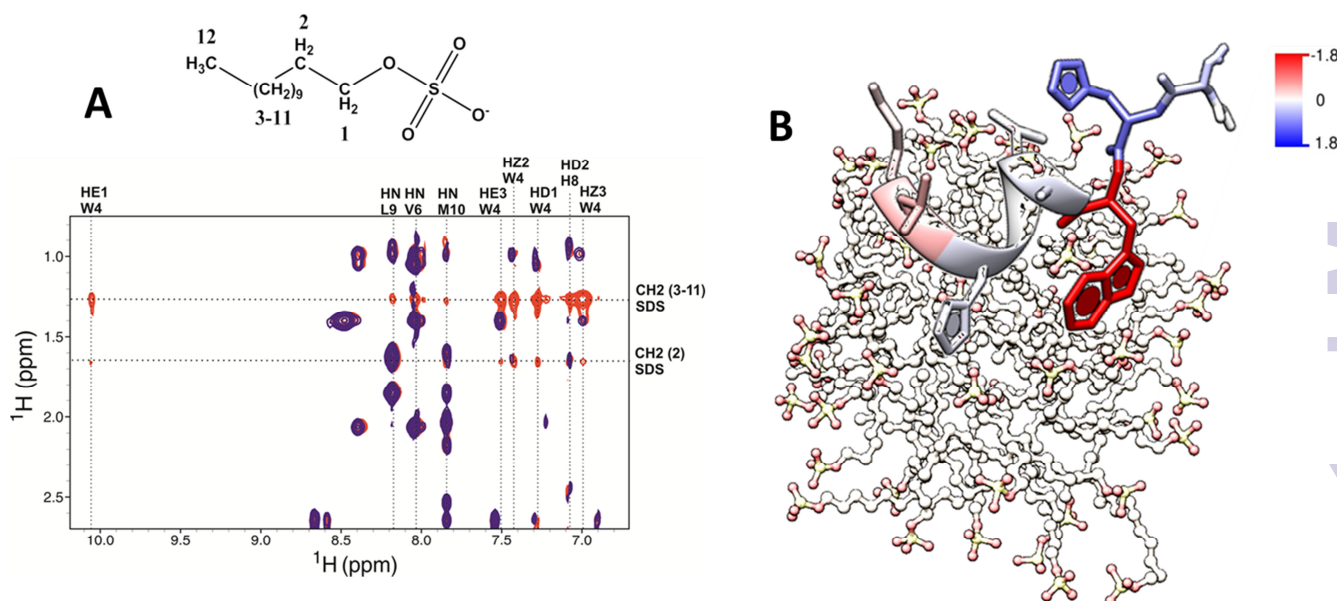


Figure 5. The mapping of the interactions observed between NMC and SDS micelles. (A) Overlapping of the ¹H,¹H-NOESY spectra of NMC obtained at 15°C when it was bound to SDS micelles (red) and when it was bound to d₂₅-SDS micelles (blue). The chemical structure of SDS is shown above the NMR spectra. Atoms are numbered arbitrarily. (B) Model representation of the interaction between NMC and SDS micelles. Aliphatic chains of SDS are colored in grey, while the corresponding sulfate group is colored in yellow (sulphur atoms) and red (oxygen atoms). NMC residues are colored base on the previously determined free energy transfer of each amino acid from water to lipid bilayers ($\Delta G = -1.8$ kcal/mol, red; $\Delta G = 1.8$ kcal/mol, blue).⁴⁰ His³ is colored taking the ΔG value determined for protonated His, while His⁸ is colored base the ΔG value determined for neutral His.

At pH 4.0 His side chains must be protonated -the pK_a of the imidazole protons range from 4.9 to 6.6 in micellar media³⁷-, and therefore highly unlikely to penetrate into the micelles. This has been the case for His containing peptides, where micelle insertion was only observed when the pH increased above the pK_a of His.³⁸ However, we unexpectedly detected unambiguous NOEs between H_β/H_{δ2} of His⁸ and the aliphatic methylene groups of SDS (Figure 5A and S5) (Table 2), which proves that His⁸ inserts into the micelles even at pH 4.0. This could only occur if the insertion occurs together with His⁸ deprotonation. In fact, the H_{δ2} and H_{ε2} chemical shift values (highly sensitive to imidazole protonation state) in His⁸ are shifted upfield upon micelle binding in a range comparable to that observed during the pH-induced deprotonation (i.e. ~0.2 ppm for H_{δ2} and ~0.4 ppm for H_{ε2}).^{38,39} This was not the case for His³, since its H_{δ2} and H_{ε2} values only underwent a slight downfield shift upon micelle binding (Table 3).

Our data indicate that NMC binds to SDS micelles only through the insertion of its C-terminal region, while the N-terminal tail remains out of the micelle (Figure 5B). This is additionally supported by the upfield chemical shifts of the C-terminal amide, whereas the chemical shifts corresponding to the amide side chain of Asn² remain unaltered (Table 3)(Figure 4B). The binding process occurs through the energetically favored insertion of Trp⁴, Val⁶, Gly⁷, Leu⁹

and Met¹⁰ (all of them with $\Delta G < 0$ of transfer from water to lipid bilayers⁴⁰), which must energetically compensate the deprotonation and the further insertion of His⁸ into the micelle (Figure 5B).

Table 3. Chemical shift values of imidazolinic protons of His³ and His⁸ and of the C-terminal and Asn² amide group atoms when NMC is either free or bound to SDS micelles.

	H _{δ2} ^[a]	H _{ε1} ^[a]	N ^[a]	H ₁ ^[a]	H ₂ ^[a]
His ³ in free NMC	7.08	8.42	--	--	--
His ³ in micelle bound NMC	7.28	8.61	--	--	--
His ⁸ in free NMC	7.14	8.43	--	--	--
His ⁸ in micelle bound NMC	7.02	8.03	--	--	--
Asn ² side chain in free NMC	--	--	113.3	7.53	6.93
Asn ² side chain in micelle bound NMC	--	--	112.8	7.52	6.88
C-terminal amide in free NMC	--	--	108.2	7.54	7.15
C-terminal amide in micelle bound NMC	--	--	105.6	7.20	7.03

^aValues are given in ppm.

2.8 The α-helical folding and the micelle binding effects on the NMC flexibility

NMC folds upon SDS micelle interaction adopting a structure similar to that displayed at 60% TFE. This scenario gives the unique opportunity to study separately the influence of the folding and the binding effect on the NMC dynamics. Hence, we acquired the ¹⁵N

R_1 , R_2 , and HET-NOE relaxation data in aqueous solution, in presence of 60% TFE, and under its SDS micelle bound state.

In aqueous solution, R_1 and R_2 constants are lower than $1.3s^{-1}$, while all HET-NOEs are negative, both features typical of intrinsically disordered peptides (IDP).⁴¹ The addition of 60% TFE increases ~ 2 -3 times the R_1 and R_2 constants, while most of the HET-NOEs become positive as a result of the rigidity linked to the α -helix formation. These variations are even more pronounced when NMC binds to SDS micelles. In this case, R_2 increase ~ 9 times and most of the HET-NOEs display values close to 0.5, thus proving that the binding additionally constrains the α -helical NMC structure (Figure 6A-C).

The R_1 and R_2 constants obtained in aqueous solution for the Trp⁴-indol group are similar to the backbone ones. However, the HET-NOE is ~ 0.9 units higher, likely as a result of the rigidity linked to the contacts of Trp⁴-H _{δ 1},H _{ϵ 3} with Ala⁵, which must reduce the side chain dynamics. The presence of 60% TFE slightly increases the R_1 and R_2 constants, revealing that the mobility of the Trp⁴ side chain is slightly reduced upon folding. Moreover, the confinement of the indol group into the SDS micelles enlarges ~ 4 times the R_2 , thus proving that the binding also additionally constrains the mobility of the Trp⁴ side chain (Figure 6A-C).

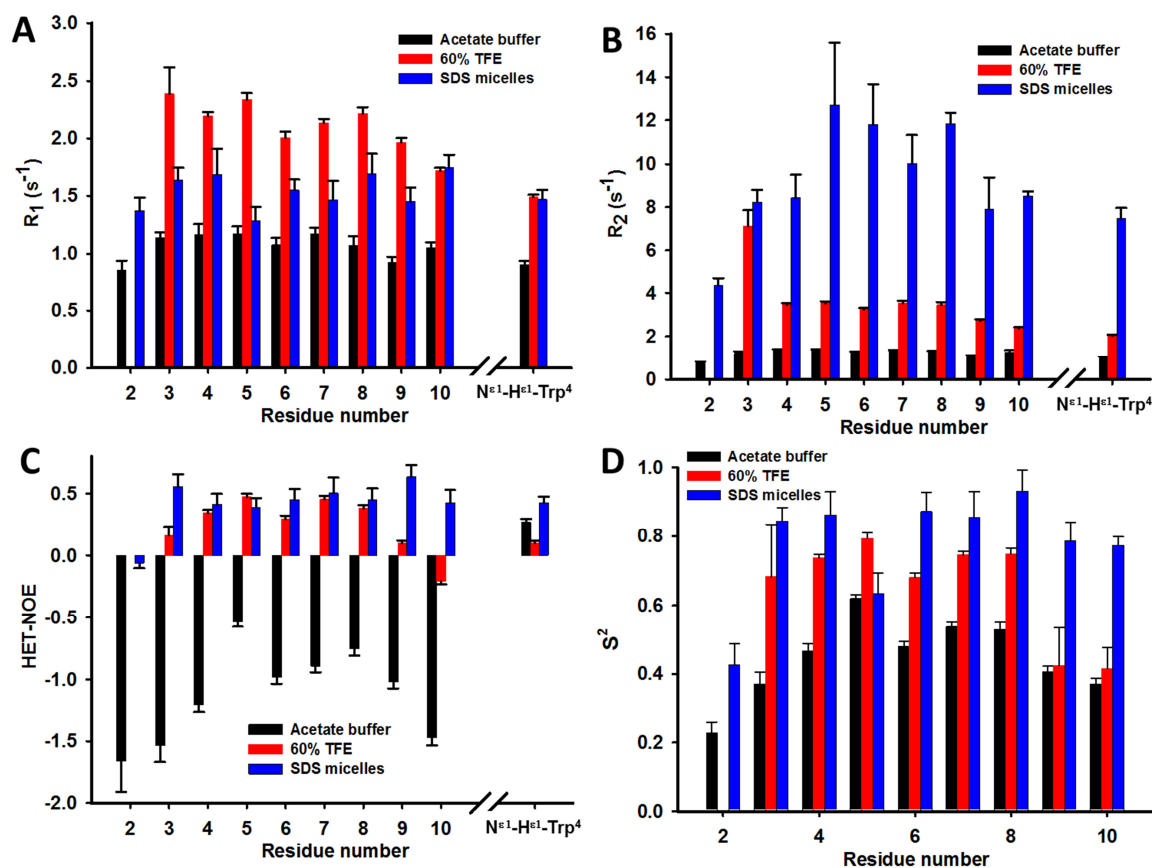


Figure 6. NMR dynamics of NMC in acetate buffer, in 60% TFE and under its micelle bound state at 14.1T and 15°C. (A-C) ¹⁵N relaxation dynamics parameters (A) R_1 , (B) R_2 and (C) heteronuclear NOE plotted as a function of the residue number. Error bars in plots indicate the curve-fit root mean square deviation of each point. Mean values are plotted as columns. (D) Order parameters (S^2) obtained from Liparizi-Szabo Model-free analysis as a function of the residue number.

The R_1/R_2 ratios within one standard deviation of the mean were then used to determine the correlation time (τ_c) of each structural ensemble. Calculations carried out with the r2r1_tm and TENSOR 2.0 software gave similar values, being 0.8 ± 0.1 ns in buffer, 2.1 ± 0.1 ns in 60% TFE, and 6.9 ± 0.1 ns under its micelle bound state. Although the NMC molecular size scarcely changed in presence of 60% TFE (Figure 1C), the τ_c increased ~ 3 times as a result of the enlarged viscosity of the TFE/water mixture.⁴² Furthermore, the τ_c of the NMC-SDS micelle complex is ~ 8 times bigger than that of free NMC, which can be ascribed to the resulting high molecular weight complex. In addition, this τ_c value is also ~ 1 ns bigger than that of free SDS micelles,⁴³ which points to the formation of 1:1 NMC-SDS micelle complex.

The backbone R_1 and R_2 values and the energy-minimized representative conformers of each NMR-derived solution structure

were used to estimate the diffusion tensor (D_{\parallel}/D_{\perp}) by using the isotropic, axially symmetric and fully anisotropic diffusion models in the software Quadratic-Diffusion.⁴⁴ The D_{\parallel}/D_{\perp} values obtained for NMC were 1.2 in buffer, 0.98 in 60% TFE, and 0.8 under its micelle bound state. Hence, the diffusion model that best describes the NMC rotational behavior under these experimental conditions is the isotropic one ($D_{\parallel}/D_{\perp} < 1.3$).

The ¹⁵N-relaxation parameters were then analyzed assuming an isotropic rotational diffusion model and according to the Liparizi-Szabo model-free formalism⁴⁵ (Tables S2-S4). The order parameters (S^2 ; indicative of the amplitude of internal ps-ns timescale motions) of NMC in water have an average value of 0.45 ± 0.12 , being within the typical range found in IDP ($S^2_{av} \sim 0.3-0.6$).^{46,47} However, the S^2 values are not homogeneous along the NMC sequence. The S^2_{av} of the residues between Trp⁴-His⁸ is notably higher than that arising

from the three N-terminal and the two C-terminal residues ($\Delta S_{av}^2 \sim 0.18$) (Figure 6D). This striking variation clearly proves that central amino acids, although integrated within the fully disordered NMC structure, display much slower motions than the terminal ones, likely as result of their inter-residual interactions.

The acquisition of the α -helical structure in the presence of 60% TFE reduced with $\sim 46\%$ the flexibility of the central residues (His³-His⁸) as evidence the $\Delta S_{av}^2 \sim 0.23$. This was not the case for the still unstructured two C-terminal residues, whose mobility was nearly unaltered upon folding of the Ala⁵-His⁸ stretch ($\Delta S_{av}^2 \sim 0.03$). The insertion of the folded NMC into SDS micelles additionally reduced the mobility of the central amino acids (His³-His⁸) with $\sim 20\%$ ($\Delta S_{av}^2 \sim 0.1$), while that corresponding to the C-terminal Leu⁹ and Met¹⁰ was reduced with $\sim 90\%$ ($\Delta S_{av}^2 \sim 0.36$) as a result of their confinement into the SDS micelle (Figure 6D).

Our results reveal that NMC in aqueous solution displays highly different conformational motions along its sequence. Moreover, the NMC α -helical folding markedly reduces the mobility of the central residues, affecting the peptide flexibility in a larger extend than the subsequent structural confinement into SDS micelles.

3 Discussion

NMC modulates different physiological processes, such as feeding or tumor growth mostly through its interaction with the BB₂R. Although its physiological implications are known since four decades,^{3,6,11} its structural features, either in its free form or when bound to the BB₂R have not yet been reported. Here we have combined different biophysical techniques to study the structural and dynamical preferences of NMC in aqueous solution and under its SDS micelle bound state. In addition, we have also analyzed the structure of NMC at different TFE/water ratios to decode the NMC folding pathway. TFE is known to induce polypeptide folding in the sense that it deprives peptides of establishing hydrogen bonds with the water thereby favouring intra-peptide hydrogen bonding.⁴⁸

Most of the small peptides do not behave as pure random coils because their residues usually do not sample all sterically accessible regions, but rather exhibit local structural preferences.⁴⁹ Hence, we used NMR to gain residue insights on the structural preferences of NMC in aqueous solution. The ¹⁵N-HSQC spectrum only display nine signals proving that either there is a main conformational state or that the dynamic equilibrium between different conformers is in a fast exchange regime (Figure 2A). This agrees with our REMD prediction of a low energy structure among the different NMC conformers.²⁴ The NMR ensemble possesses a well-defined backbone architecture resembling a distorted S (Figure 1C), which is built through short range contacts between the central residues. We already predicted these turns using REMD, since $\sim 20\%$ of the sampling displayed the segment Trp⁴-Gly⁷ stabilized by a hydrogen bond. In addition, others turns like His³-Trp⁴, Trp⁴-Ala⁵ or Gly⁷-His⁸ were only $\sim 10\%$ sampled.²⁴ This S-like architecture is also adopted in NMC-Ni²⁺ complex since two turns are formed, one involving the three first residues coordinating the metal and the other linking Ala⁵ to His⁸.²²

NMC folds into a helical structure upon increasing the TFE percentage as result of the reduction of the dielectric constant that favors the formation of intramolecular hydrogen bonds. However, the ease to adopt this α -helical structure is not the same along the entire sequence. The presence of 10% TFE only induces the stretching of the C-terminal region that folds back into a helical-like structure only when TFE rises up to 25%. The C-terminal helical structuration is finally strengthened at 40% TFE and it does not further change at 60 or 90% TFE. The N-terminal segment is more resistant to undergo the coil-helix transition, since it only acquires a helical-like structure when the TFE content is 60%, becoming fully α -helical 90%.

Additionally we studied the molecular complex formed between NMC and SDS micelles. ITC was used to characterize the binding process. Initially it appeared a highly exothermic event proportional to the NMC concentration and attributed to electrostatic interactions.^{31,33} This evidenced that NMC is the limiting reactant in this region of the plot and that the binding is notably weak. NMC started to bind SDS at a *cac* of ~ 3.3 mM, consistent with what was observed when using hydrophobically alkali-soluble emulsion polymers (HASE) (*cac* ~ 4 mM).⁵⁰ *Cac* was independent of the NMC or HASE concentration, although it is concentration-dependent in folded proteins.³³ The binding saturation of NMC occurred at [SDS] ~ 4 mM, which agrees with the *cmc* of SDS at 15°C,²⁹ and it did not change with the NMC concentration, thus differing of what occurs in folded proteins.³³ The SDS added beyond the *cmc* remains in micellar form and leads to an asymptotic curve that is related to the NMC hydrophobicity.^{34,50} Its $\alpha_{\Delta H}$ value is ~ 86 kJ/mol-mM lower than that determined for the electrostatic interactions between NMC and SDS monomers, which proves that the driving force leading to the NMC/SDS micelle binding (likely hydrophobic) is weaker than an electrostatic one. This $\alpha_{\Delta H}$ is also ~ 15 times lower than that determined for folded proteins,³³ which must account for the low hydrophobicity of NMC in comparison to larger polypeptides. The formation of micelles alone or in presence of NMC was always thermodynamically favored through an entropy-driven process. Moreover, the calculation of ΔG_{ps} (which compares the stability of the interactions between NMC-SDS and SDS-SDS) demonstrated that the NMC-SDS was only ~ 1 kJ/mol more favored than the SDS-SDS interaction, being weaker than what was determined for HASE-SDS interactions (~ 4 kJ/mol).⁵⁰

Next, we calculated the solution structure of NMC under its micelle bound state and we characterized the architecture of the complex. Although it was predicted that the replacement of Leu³ in NMB by His³ in NMC would hinder the acquisition of a helical membrane-bound structure,²⁰ we have shown that the C-terminal region of NMC folds into an α -helix upon micelle insertion, whereas the N-terminal segment remains unstructured. This folding process must be directly related with the energetically favored insertion of Trp⁴, Val⁶, Gly⁷, Leu⁹ and Met¹⁰ (residues with a $\Delta G < 0$ of transfer from water to lipid bilayers⁴⁰) into the non-polar micelle, which was experimentally observed through intermolecular NOEs (Figure 5). However, this hydrophobic insertion cannot occur without the enclosure of His⁸ into the micelle, which is expected to be fully protonated at pH 4.0, and therefore highly unfavorable. Nevertheless, NMR data reveals that His⁸ but not His³ deprotonates

during the NMC insertion. These observations enabled us to hypothesize that the favorable hydrophobic interactions of the residues near His⁸ would energetically compensate its unfavorable deprotonation and insertion. This idea is also supported by the small ΔG_{ps} value of the NMC-SDS complex in comparison to other peptide-SDS complexes.⁵⁰

The micelle bound NMC structure displays Trp⁴, His⁸ and Leu⁹ oriented toward the same face. These residues correlate with Trp⁸, His¹² and Leu¹³ in bombesin, which are essential for the binding to the bombesin family receptors.⁵¹ Hence, it is likely that Trp⁴, His⁸ and Leu⁹ also reorient as NMC approaches to its receptor, which further validates the micelle-bound NMC structure, also within a biologically relevant context.

The ability of NMC to form a short α -helix during its micelle insertion may result in conformation and/or orientation-selective interactions. Hence, the wide spectrum of similar but not identical biological activities of bombesin-related peptides raises the possibility that fluctuations of secondary structure can modulated their accessibility to different receptors, a mechanism already proven for neurokinins and opioid peptides.⁵² Hence, we have completed our structural data analyzing the dynamics of NMC in water, in presence of 60% TFE and under its micelle bound state. The fact that NMC at 60% TFE displays a structure similar to that adopted when it is embedded into micelles has allowed us to discriminate the folding and the binding effects on the molecular tumbling and dynamics.

The R_1/R_2 ratios were used to determine the τ_c values, which represent the time of the molecule to tumble in function of the size, shape and viscosity. The τ_c of NMC in water is similar to that found for other peptides of similar size.⁵³ The addition of 60% TFE enlarged the τ_c \sim 3 times, which is attributed to an increased solvent viscosity typical of the TFE/water mixtures⁴² and not to changes in the peptide size.^{53,54} The τ_c of the NMC-SDS complex was \sim 1ns bigger than that of free SDS micelles proving that the NMC slightly reduces the micellar tumbling rate as a result of the formation of 1:1 complex; the stoichiometry mainly observed in peptide-micelle complexes.^{46,55}

¹⁵N relaxation data was used to determine the diffusion tensor of NMC in water, at 60% TFE and under its micelle-bound state. All the D_{\parallel}/D_{\perp} values were <1.3 , thus suggesting an isotropic rotational behavior. This model has already been adopted to study the dynamics of other small peptides, either in their free form⁵⁶ or under their micelle-bound states.⁴⁶ NMC dynamics were studied applying the model-free approach,⁴⁵ which fits the relaxation data to one of the five models characteristic of the complexity of the residue level dynamics. The 9 residues of NMC in water were described by the model 2, indicating internal motions (τ_e) on ps-ns timescales. This was also the case for most of the residues of NMC at 60% TFE, except His³ that was fitted to model 4, and Leu⁹/Met¹⁰ that were fitted to model 5, hence suggesting complex internal motions. Five out of the nine residues in the NMC-SDS complex were fitted to model 1, proving their lack of flexibility (Tables S2-S4).

Residue level mobility was qualitatively compared within the same NMC structure and between the three different NMC structures

through the analysis of S^2 . Folded proteins exhibit $S^2_{av} \sim 0.8$, while mobile terminal residues display a $S^2_{av} \sim 0.6$ ⁵⁷ similar to IDPs ($S^2_{av} \sim 0.3-0.6$).^{46,47} The S^2_{av} of NMC in water was within the typical range of IDPs. However, the S^2 values notably changed between the central and the terminal residues, pointing towards a constrained mobility of the central residues, a trend also observed at 60% TFE. S^2 values also revealed that the formation of intramolecular hydrogen bonds linked to the α -helical folding reduces much more the backbone flexibility than the intermolecular hydrophobic interactions associated to the insertion of NMC into the SDS micelles. Hence, the coil-helix transition has a higher impact on the dynamics than the NMC confinement.

The ¹⁵N-relaxation data acquired at 60% TFE could be affected by the increase in the viscosity ($\Delta\eta \sim 1\text{cp}$ at 25°C⁴²). However, data comparing the NMR dynamics of the *Escherichia coli* orthologue of frataxin (CyaY) in water ($\eta \sim 0.89\text{cp}$ ⁴²) and in hen egg white ($\eta \sim 4\text{cp}$ ⁵⁸), prove that viscosity does not affect the CyaY fold nor the HET-NOE values, but notably decreased and increased the R_1 and R_2 values, respectively.⁵⁹ The viscosity change scarcely affected the S^2 values of CyaY, calculated assuming an axially symmetric diffusion model ($\Delta S^2_{av} \sim 0.06$) (Figure S6). Contrarily, R_1 , R_2 , HET-NOE and S^2 values of NMC notably enhanced when ongoing from pure water to 60% TFE, thus proving that these changes are associated to structural alterations rather than viscosity modifications.

4 Experimental

4.1 Materials

NMC was purchased from Hölzel Diagnostika Handels GmbH. Sodium dodecyl sulfate (SDS, 99%), deuterated sodium dodecyl sulfate (d_{25} -SDS, 98%), 3-(trimethylsilyl)-1-propanesulphonic acid (DSS), deuterated (d_3 -TFE, 99.5%) and non-deuterated 2,2,2-trifluoroethanol (TFE) were acquired from Sigma-Aldrich. All reagents were used without any further purification.

4.2 Circular dichroism (CD) studies

Circular dichroism (CD) spectra of NMC were recorded on a Jasco-715 spectropolarimeter equipped with a thermostatted cell holder controlled by a Jasco Peltier element. Far-UV CD spectra were acquired from 260 to 190nm at 15°C in a 0.1cm path length quartz cuvette at a NMC concentration of 30 μ M in 10mM acetate buffer (pH 4.0) containing different percentages of TFE (0, 10, 25, 40, 60 and 90%). The CD spectrum of NMC was also obtained in a buffered aqueous solution in presence of 150mM SDS. The scan speed was 50nm/min with a response time of 1s and a step resolution of 0.2nm, while 15 scans were accumulated. Base-line spectra were subtracted for all spectra. The secondary structure content was derived from the far-UV CD spectra by using the BeStSel on-line platform (<http://bestsel.elte.hu/>).

4.3 Sample preparation for NMR studies

A 5mM NMC solution was prepared in 10mM acetate buffer at pH 4.0 containing 10% of D₂O and 1.6mM of DSS (added as internal reference). This solution was additionally prepared in the depicted

acetate buffer but in presence of 10, 25, 40, 60 or 90% d_3 -TFE (to study the NMC folding pathway upon addition of a structuring solvent), in presence of 150mM d_{25} -SDS (to determine the NMC structure bound to SDS micelles), and in presence of 50mM SDS (to map the intermolecular interactions occurring between NMC and SDS micelles).

4.4 NMR spectroscopy

NMR experiments were carried out at 15°C on a Bruker Avance III spectrometer operating at 14.1T (600MHz) and equipped with a 5-mm ^{13}C , ^{15}N , ^1H triple resonance cryoprobe. For sequence-specific assignments ^1H , ^1H -TOCSY experiments⁶⁰ were performed with the MLEV-17 spin-mixing pulse using a mixing time of 80ms. The ^1H , ^1H -NOESY experiments⁶¹ were acquired with a mixing time of 500ms for the samples containing different d_3 -TFE/water ratios, while a mixing time of 200ms was used for the samples containing SDS micelles. 2D ^{15}N -HSQC and ^{13}C -HSQC spectra were also acquired at natural abundance. Spectra were obtained with 2048 data points x 512 increments and with a spectral width of 7184Hz in both dimensions. Water suppression was achieved by the field-gradient method with WATERGATE sequence.⁶² ^1H and ^{13}C chemical shifts were measured relative to the methyl resonance of internal DSS at 0ppm. ^{15}N chemical shifts were referenced indirectly using the ^1H , X frequency ratios of the zero-point. The relative diffusion coefficients (D) of NMC were measured by the pulse field gradient spin echo (PGSE) using standard ledbpgp2s experiment.⁶³ D is a good indicator of the molecular mobility that is relative to the viscosity and to the molecular size. All the spectra were processed using NMRPipe/NMRDraw,⁶⁴ analyzed by Xeasys/Cara⁶⁵ and plotted using Sparky software.⁶⁶

4.5 NMR structure calculations

The NMR experiments permitted to assign the resonance frequencies of ^{13}C , ^1H and ^{15}N of NMC. The assignments were then used to calculate the secondary structure propensity (SSP) scores⁶⁷ (<http://pound.med.utoronto.ca/software.html>). The SSP score is the weighted average of the chemical shifts from different nuclei in a given residue, with the relative weighting reflecting the sensitivity of different secondary shifts to structure. An SSP score of 1.0 suggest a fully formed α -helix, a -1.0 value indicates a β -strand, while a 0 score specifies a random coil conformation. The chemical shift assignments were also used to obtain the geometrical restrains resulting from the NOEs intensities, which were then used to calculate the NMC solution structures. NOE cross peak assignment was done using the automated NOE assignment of CYANA,²⁷ a software that was further used to calculate the NMC ensembles. The standard protocol was used with seven cycles of combined automated NOE assignment and structure calculation of 200 conformers in each cycle, of which the 20 structures with lowest target function value were selected for further minimization and analysis. PROCHECK-NMR⁶⁸ was used to analyze the quality of the structures through the Protein Structure Validation Server (PSV) (http://psvs-1_4-dev.nesg.org/).⁶⁹ MOLMOL software⁷⁰ was used for visualization and UCSF Chimera⁷¹ was used for structural representations.

4.6 NMR relaxation measurements

^{15}N longitudinal (R_1) and transverse (R_2) relaxation data, as well as steady-state ^{15}N HET-NOE data, were acquired at 15°C in aqueous solution, in presence of 60% TFE and in presence of 150mM d_{25} -SDS. In all cases R_1 values were determined using a series of 11 experiments with relaxation delays ranging from 10 to 2000ms, while ^{15}N HET-NOE measurements were performed by 3s high power pulse train saturation within a 5s recycle delay. R_1 and ^{15}N HET-NOE data were acquired using standard pulse sequences,⁷² as well as R_2 data of the NMC solution containing d_{25} -SDS, recorded using 11 different relaxation delays ranging from 8 to 128ms. R_2 measurements of the solutions prepared in water and in 60% TFE were carried out using the pulse program recently developed by Yuwen and Skrynnikov with modifications, which permits the increase of the relaxation delays avoiding the cryoprobe heating.⁷³ In these cases, R_2 values were measured using 9 relaxation delays ranging from 58 to 691ms. Recycle delays were 3s in both, R_1 and R_2 experiments. Thirty-two scans in R_1 , R_2 and 200 scans in ^{15}N HET-NOE spectra per t_1 experiment were acquired. 2048x128 complex points were obtained during R_1 and R_2 experiments, whereas 2048x164 complex points were acquired in the ^{15}N HET-NOE experiments.

4.7 NMR relaxation analysis

R_1 and R_2 relaxation data were fitted to a mono-exponential decay function, while ^{15}N HET-NOE data was obtained as the ratio of the peaks intensities from the saturated and unsaturated spectra. Relaxation constants and experimental errors were calculated using the Protein Dynamics Center software (Bruker, Germany). R_1 and R_2 relaxation constants were then used to determine the NMC correlation times (τ_c) at each experimental condition using both, the r2r1_tm (Palmer's group, http://www.hhmi.umbc.edu/toolkit/analysis/palmer/r2r1_tm.html) and the TENSOR 2.0 software.⁷⁴ The magnitude and orientation of the rotational diffusion tensor was determined from the R_1 and R_2 relaxation constants and the energy-minimized representative conformers of the NMR-derived solution structures using the software Quadratic-Diffusion.⁴⁴

The TENSOR 2.0 was also used to calculate the generalized order parameters describing the amplitudes of internal motions (S^2). The ^{15}N relaxation constants and the energy-minimized solution structures were analyzed according to the molecular diffusion derived by Woessner in combination with the Lipari-Szabo model-free analysis of local flexibility.⁴⁵ The amide bond length was fixed at 1.02Å. Five different models were tested to characterize the internal dynamics of the NH groups:⁷⁵ model 1 (S^2), model 2 (S^2 , τ_e), model 3 (S^2 , R_{ex}), model 4 (S^2 , τ_e , R_{ex}) and model 5 (S_f^2 , S_s^2 , τ_e). τ_e is the effective internal correlation time (describes motions on timescale >20ps), R_{ex} is a chemical exchange term (describes slow timescale motions on the order of μs -ms), and S_f^2 and S_s^2 are terms that result from splitting the generalized order parameter into two order parameters reflecting slower and faster motions, respectively. The confidence levels were estimated using 100 Monte Carlo simulations per run in combination with χ^2 and F -test criteria.

4.8 Fluorescence measurements

The intrinsic fluorescence spectra of NMC were acquired at 15°C on a Varian Cary Eclipse fluorimeter equipped with a Peltier-controlled cell holder. Emission spectra were obtained between 300 and 400nm using an excitation wavelength of 280nm. The fluorescent spectra were collected using a 0.1mM NMC solution in 10mM acetate buffer at pH 4.0, either alone or in presence of 50mM of SDS. The change in the solvent accessible surface area of Trp⁴ was measured by acrylamide quenching experiments, which permitted the calculation of the corresponding Stern-Volmer constants (K_{sv}). Aliquots of a 1M acrylamide aqueous solution were added to the cuvette containing either the peptide alone or the peptide/SDS mixture. Emission spectra were collected as previously described after each addition of the quencher. The K_{sv} values were calculated from the following equation,

$$F_0/F = 1 + K_{sv}[Q] \quad (1)$$

where F_0 is the initial fluorescence of the peptide and F is the fluorescence intensity following the addition of soluble quencher, Q .

4.9 Isothermal titration calorimetry (ITC) measurements

ITC experiments were used to measure the thermodynamics parameters of the NMC-SDS interaction. ITC measurements were carried out on a Nano-ITC (TA Instruments©) at 15°C in duplicate. In a typical experiment, the sample cell (190µl) was filled with 10mM acetate buffer (pH 4.0) in absence or in presence of different NMC concentrations (i.e. 10µM, 20.8µM, 42µM and 62.5µM) and stirred at 250rpm, while a 35mM SDS buffered solution was loaded in the injection syringe. Both solutions were degassed before use. SDS solution was titrated into the sample cell as a sequence of 32 injections (the first four injections of 2µl and the other injections of 1.5µl). The time between successive injections was 400s. Raw data corresponding to the heating rate (µJ/s) was integrated to obtain the observed molar enthalpy change (ΔH) at each SDS concentration. The data corresponding to the titration of SDS into acetate buffer was subtracted to the data corresponding to the titration of SDS into a NMC buffered solution before the analysis of the ΔH variation. Titration of acetate buffer into a NMC buffered solution resulted in small ΔH variations that were not further considered in the data analysis. All data acquisition and analysis were performed using NanoAnalyze software.

The Gibbs free energy changes of aggregation (ΔG_{mic}) and aggregation in presence of NMC (ΔG_{ag}) were calculated from the ITC data through the application of the charged phase separation and mass-action models (Eq. 2).³⁵

$$\Delta G_{mic/ag} = (1+K)RT \ln [cac \text{ or } cmc] \quad (2)$$

A factor of (1+K) is needed to calculate the free energy of ionic SDS, where K is the micellar charge fraction with a value of 0.85.⁷⁶ The enthalpy change and free energy changes were also used to calculate the entropy changes of micellization (ΔS_{mic}) and aggregation in presence of NMC (ΔS_{ag}).

5 Conclusions

The results reported in this work allow a rationalization of the structural determinants of NMC in aqueous solution, and describe the different folding steps that potentially occur during its interaction with its natural partners. The description of the NMC-SDS micelle complex revealed that the hydrophobic binding must energetically compensate the deprotonation and the micelle insertion of His⁸, which results into a low ΔG of interaction. The fact that the solution structure of NMC at 60% TFE mimics the micelle-bound structure provides an excellent opportunity to discriminate the folding and the binding effects on the NMC mobility. We have observed that the folding constrains the NMC mobility twofold more than its micelle confinement. Our data contribute to the general understanding of the mechanisms involving peptide-lipids interactions, and provide fundamental to insights into the structure-flexibility relationship of bombesin-like peptides. The novel insights into the binding-induced folding mechanism of NMC also constitute a new molecular platform for the future design of antagonists of the bombesin family receptors.

Acknowledgements

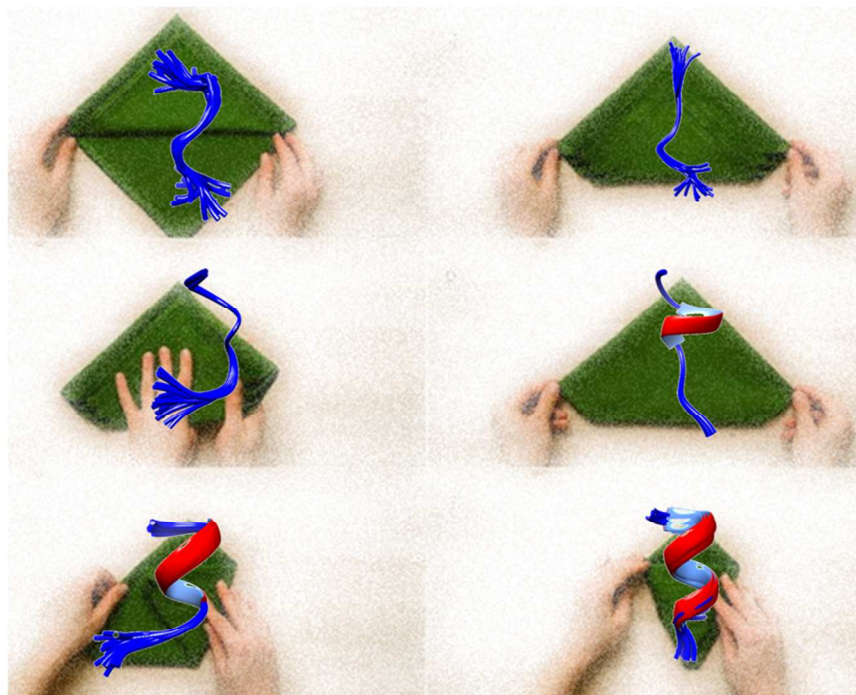
The authors are grateful for the excellent technical assistance from the Serveis Científicotècnics at the UIB, especially to Dr. Joan Cifre for his generous assistance with ITC measurements. K.P. is supported by a FWO Pegasus long-term post-doctoral fellowship (1218713). P.S. is supported by a post-doctoral fellowship (PD/009/2013) from the Conselleria d'Educació, Cultura i Universitats of the Balearic Government, and the European Social Fund through the ESF Operational Program of the Balearic Islands 2013-2017. This work is supported by the project AAEE26/2014 from the Conselleria d'Educació, Cultura i Universitats of the Balearic Government, and FEDER funded.

References

- 1 H. Ohki-Hamazaki, M. Iwabuchi and F. Maekawa, *Int. J. Dev. Biol.*, 2005, **49**, 293.
- 2 A. Anastasia, V. Erspamer and M. Bucci, *Experientia*, 1971, **27**, 166.
- 3 N. Minamino, K. Kangawa and H. Matsuo, *Biochem. Biophys. Res. Commun.*, 1984, **119**, 14.
- 4 R. T. Jensen, J. F. Battey, E. R. Spindel and R. V. Benya, *Pharmacol. Rev.*, 2008, **60**, 1.
- 5 T. H. Moran, T. W. Moody, A. M. Hostetler, P. H. Robinson, M. Goldrich and P. R. McHugh, *Peptides*, 1988, **9**, 643; E. E. Ladenheim, R. T. Jensen, S. A. Mantey and T. H. Moran, *Brain Res.*, 1993, **593**, 168.
- 6 A. Guglietta, C. L. Strunk, B. J. Irons and L. H. Lazarus, *Peptides*, 1985, **6 Suppl 3**, 75.
- 7 T. Reynolds and R. D. Pinnock, *Brain Res.*, 1997, **750**, 67.
- 8 T. Tachibana, K. Matsuda, H. Sawa, A. Mikami, H. Ueda and M. A. Cline, *Gen. Comp. Endocrinol.*, 2010, **169**, 144; T. Tachibana, K. Matsuda, S. I. Khan, H. Ueda and M. A. Cline, *Comp. Biochem. Physiol. A Mol. Integr. Physiol.*, 2010, **156**, 394.
- 9 E. M. Fekete, E. E. Bagi, K. Tóth and L. Lénárd, *Brain Res Bull.*, 2007, **71**, 386.

- 10 H. Zhao, S. Matsuda, S. Thanthan, S. Yannaing and H. Kuwayama, *Peptides*, 2012, **37**, 194.
- 11 F. Cuttitta, D. N. Carney, J. Mulshine, T. W. Moody, J. Fedorko, A. Fischler and J. D. Minna, *Nature*, 1985, **316**, 823.
- 12 D. B. Cornelio, R. Roesler and G. Schwartzmann, *Ann. Oncol.*, 2007, **18**, 1457.
- 13 W. Guojun, G. Wei, O. Kedong, H. Yi, X. Yanfei, C. Qingmei, Z. Yankai, W. Jie, F. Hao, L. Taiming, L. Jingjing and C. Rongyue, *Endocr. Relat. Cancer*, 2008, **15**, 149.
- 14 M. Sioud and A. Mobergslien, *Biochem. Pharmacol.*, 2012, **84**, 1123.
- 15 I. D. Majumdar and H. C. Weber, *Curr. Opin. Endocrinol. Diabetes Obes.*, 2012, **19**, 3.
- 16 G. Schwartzmann, L. P. DiLeone, M. Horowitz, D. Schunemann, A. Cancelli, A. S. Pereira, M. Richter, F. Souza, A. B. da Rocha, F. H. Souza, P. Pohlmann and G. de Nucci, *Invest. New Drugs*, 2006, **24**, 403.
- 17 D. C. Damin, F. S. Santos, R. Heck, M. A. Rosito, L. Meurer, L. M. Kliemann, R. Roesler and G. Schwartzmann, *Dig. Dis. Sci.*, 2010, **55**, 2203.
- 18 B. A. Nock, R. Cescato, E. Ketani, B. Waser, J. C. Reubi and T. Maina, *J. Med. Chem.*, 2012, **55**, 8364.
- 19 T. Maina, B. A. Nock and S. Mather, *Cancer Imaging.*, 2006, **6**, 153.
- 20 D. Erne and R. Schwyzer, *Biochemistry*, 1987, **26**, 6316.
- 21 E. Polverini, P. Neyroz, P. Fariselli, R. Casadio and L. Masotti, *Biochem. Biophys. Res. Commun.*, 1995, **214**, 663.
- 22 G. Gasmi, A. Singer, J. Forman-Kay and B. Sarkar, *J. Peptide Res.*, 1997, **49**, 500.
- 23 C. Harford and S. Bibudhendra, *Biochem. Biophys. Res. Commun.*, 1995, **209**, 877.
- 24 P. Sharma, P. Singh, K. Bisetty, A. Rodriguez and J. J. Perez, *J. Pept. Sci.*, 2011, **17**, 174.
- 25 M. Buck, *Q. Rev. Biophys.*, 1998, **31**, 297; E. R. G. Main and S. E. Jackson, *Nat. Struct. Biol.*, 1999, **6**, 831.
- 26 S. Espinosa, E. Bosch, M. Rosés and K. Valkó, *J. Chromatogr. A*, 2002, **954**, 77.
- 27 J. G. Jee and P. Güntert, *J. Struct. Funct. Genom.*, 2003, **4**, 179; T. Herrmann, P. Güntert and K. Wüthrich, *J. Mol. Biol.*, 2002, **319**, 209.
- 28 G. Merutka, H. J. Dyson and P. E. Wright, *J. Biomol. NMR*, 1995, **5**, 14.
- 29 A. Wangsakan, P. Chinachoti and D. J. McClements, *Food Hydrocolloid.*, 2006, **20**, 461.
- 30 Z. Király and I. Dekány, *J. Colloid Interf. Sci.*, 2001, **242**, 214.
- 31 M. D. Lad, V. M. Ledger, B. Briggs, R. J. Green and R. A. Frazier, *Langmuir*, 2003, **19**, 5098.
- 32 C. Trandum, P. Westh, K. Jorgensen and O. G. Mouritsen, *Biophys. J.*, 2000, **78**, 2486.
- 33 M. M. Nielsen, K. K. Andersen, P. Westh and D. E. Otzen, *Biophys. J.*, 2007, **92**, 3674.
- 34 G. Wang and G. Olofsson, *J. Phys. Chem.*, 1995, **99**, 5588.
- 35 B. Lindman, K. Thalberg in *Interactions of surfactants with Polymers and Proteins*, (Eds.: E. D. Goddard, K. P. Ananthapadmanabhan), CRC Press, Boca Raton, FL, 1993, p 203.
- 36 K. Polewski, *Biochim. Biophys. Acta*, 2000, **1523**, 56; E. F. Haney, F. Lau and H. J. Vogel, *Biochim. Biophys. Acta*, 2007, **1768**, 2355.
- 37 B. Bechinger, *J. Mol. Biol.*, 1996, **263**, 768.
- 38 J. Georgescu, V. H. Munhoz and B. Bechinger, *Biophys. J.*, 2010, **99**, 2507; C. Aisenbrey, R. Kinder, E. Goormaghtigh, J. M. Ruyschaert and B. Bechinger, *J. Biol. Chem.*, 2006, **281**, 7708.
- 39 D. H. Sachs, A. N. Schechter and J. S. Cohen, *J. Biol. Chem.*, 1971, **246**, 6576.
- 40 W. C. Wimley and S. H. White, *Nat. Struct. Biol.*, 1996, **3**, 842.
- 41 A. T. Alexandrescu, K. Rathgeb-Szabo, K. Rumpel, W. Jahnke, T. Schulthess and R. A. Kammerer, *Protein Sci.*, 1998, **7**, 389; T. Mittag, S. Orlicky, W. Y. Choy, X. Tang, H. Lin, F. Sicheri, L. E. Kay, M. Tyers and J. D. Forman-Kay, *Proc. Natl. Acad. Sci. U.S.A.*, 2008, **105**, 17772; R. Kiss, D. Kovács, P. Tompa and A. Perczel, *Biochemistry*, 2008, **47**, 6936.
- 42 G. Gente and C. la Mesa, *J. Sol. Chem.*, 2000, **29**, 1159.
- 43 K. Lycknert, T. Rundlöf and G. Widmalm, *J. Phys. Chem. B*, 2002, **106**, 5275.
- 44 L. K. Lee, M. Rance, W. J. Chazin and A. G. Palmer, *J. Biomol. NMR*, 1997, **9**, 287.
- 45 G. Lipari and A. Szabo, *J. Am. Chem. Soc.*, 1982, **104**, 4546.
- 46 S. M. Patil, S. Xu, S. R. Sheftic and A. T. Alexandrescu, *J. Biol. Chem.*, 2009, **284**, 11982.
- 47 J. B. Duvignaud, C. Savard, R. Fromentin, N. Majeau, D. Leclerc and S. M. Gagné, *Biochem. Biophys. Res. Commun.*, 2009, **378**, 27; A. V. Buevich, U. P. Shinde, M. Inouye and J. Baum, *J. Biomol. NMR*, 2001, **20**, 233; T. S. Ulmer and A. Bax, *J. Biol. Chem.*, 2005, **280**, 43179.
- 48 D. Roccatano, G. Colombo, M. Fioroni and A. E. Mark, *Proc. Natl. Acad. Sci. U.S.A.*, 2002, **99**, 12179.
- 49 R. Schweitzer-Stenner, *Mol. Biosyst.* **2012**, **8**, 122.
- 50 W. P. Seng, K. C. Tam, R. D. Jenkins and D. R. Bassett, *Macromolecules*, 2000, **33**, 1727.
- 51 D. C. Horwell, W. Howson, D. Naylor, S. Osborne, R. D. Pinnock, G. S. Ratcliffe and N. Suman-Chauhan, *Int. J. Pept. Protein Res.*, 1996, **48**, 522.
- 52 R. Schwyzer, *Biochemistry*, 1986, **25**, 6335.
- 53 M. Ramirez-Alvarado, V. A. Daragan, L. Serrano and K. H. Mayo, *Protein Sci.*, 1998, **7**, 720; D. Idiyatullin, A. Krushelnitsky, I. Nesmelova, F. Blanco, V. A. Daragan, L. Serrano and K. H. Mayo, *Protein Sci.*, 2000, **9**, 2118.
- 54 P. Kaczka, M. Winiewska, I. Zhukov, B. Rempola, K. Bolewska, T. Łoziński, A. Ejchart, A. Poznańska, K. L. Wierzchowski and J. Poznański, *Eur. Biophys. J.*, 2014, **43**, 581.
- 55 A. Perdih, A. R. Choudhury, Š. Župerl, E. Sikorska, I. Zhukov, T. Solmajer and M. Novič, *PLoS One*, 2012, **7**, e38967.
- 56 M. Wang, M. Prorok and F. J. Castellino, *Biophys. J.*, 2010, **99**, 302.
- 57 J. L. Goodman, M. D. Pagel and M. J. Stone, *J. Mol. Biol.*, 2000, **295**, 963.
- 58 E. Robinson-Lang and C. Rha, *Int. J. Food Sci. Technol.*, 1982, **17**, 595.
- 59 G. Martorell, M. Adrover, G. Kelly, P. A. Temussi and A. Pastore, *Proteins*, 2011, **79**, 1408.
- 60 A. Bax, and D. G. Davis, *J. Magn. Reson.*, 1985, **65**, 355.
- 61 A. Kumar, R. R. Ernst and K. Wüthrich, *Biochem. Biophys. Res. Commun.*, 1980, **95**, 1.
- 62 M. Piatto, V. Saudek and V. Sklenar, *J. Biomol. NMR*, 1992, **2**, 661.
- 63 D. Wu, A. Chen and C. S. Johnson Jr., *J. Magn. Reson. A*, 1995, **115**, 260.
- 64 F. Delaglio, S. Grzesiek, G. W. Vuister, G. Zhu, J. Pfeifer and A. Bax, *J. Biomol. NMR*, 1995, **6**, 277.
- 65 C. Bartels, T. H. Xia, M. Billeter, P. Güntert and K. Wüthrich, *J. Biomol. NMR*, 1995, **6**, 1.
- 66 T. D. Goddard, D. G. Kneller, SPARKY 3. University of California, San Francisco, CA, USA. 2008.
- 67 J. A. Marsh, V. K. Singh, Z. Jia and J. D. Forman-Kay, *Protein Sci.*, 2006, **15**, 2795.
- 68 R. A. Laskowski, J. A. Rullmann, M. W. MacArthur, R. Kaptein and J. M. Thornton, *J. Biomol. NMR*, 1996, **8**, 447.
- 69 A. Bhattacharya, R. Tejero, G. T. Montelione, *Proteins*, 2001, **66**, 778.
- 70 R. Koradi, M. Billeter and K. Wüthrich, *J. Mol. Graph.*, 1996, **14**, 51.

- 71 E. F. Pettersen, T. D. Goddard, C. C. Huang, G. S. Couch, D. M. Greenblatt, E. C. Meng and T. E. Ferrin, *J. Comput. Chem.*, 2004, **25**, 1605.
- 72 N. A. Farrow, R. Muhandiram, A. U. Singer, S. M. Pascal, C. M. Kay, G. Gish, S. E. Shoelson, T. Pawson, J. D. Forman-Kay and L. E. Kay, *Biochemistry*, 1994, **33**, 5984.
- 73 T. Yuwen and N. R. Skrynnikov, *J. Mag. Res.*, 2014, **241**, 155.
- 74 P. Dossset, J. C. Hus, M. Blackledge, D. Marion, *J. Biomol. NMR*, 2000, **16**, 23.
- 75 V. A. Jarymowycz and M. J. Stone, *Chem. Rev.*, 2006, **106**, 1624.
- 76 J. R. Lu, A. Marrocco, T. J. Su, R. K. Thomas and J. Penfold, *J. Colloid. Interface Sci.*, 1996, **178**, 614.



NMR has been used to elucidate the folding pathway of neuromedin C (NMC) at residue level (see figure) and to characterize the architecture of the NMC-SDS micelle complex. The C-terminal region of NMC is more prone to acquire an α -helical fold than the N-terminus. The C-terminus is also involved in the binding to SDS micelles. The NMC insertion into micelles implies its α -helical folding, which constrains the NMC flexibility more than the micelle confinement itself.

254x190mm (96 x 96 DPI)